sustainability

MDPI

Article

Reduction and Degradation of Paraoxon in Water Using Zero-Valent Iron Nanoparticles

Veronica A. Okello [1,*], Isaac O. K'Owino [2], Kevin Masika [2] and Victor O. Shikuku [3,*]

[1] Department of Physical Sciences, Machakos University, Machakos P.O. Box 136-90100, Kenya
[2] Department of Pure and Applied Chemistry, Masinde Muliro University of Science and Technology, Kakamega P.O. Box 190-50100, Kenya; ikowino@mmust.ac.ke (I.O.K.); kevin.masika@gmail.com (K.M.)
[3] Department of Physical Sciences, Kaimosi Friends University, Kaimosi P.O. Box 385-50309, Kenya
* Correspondence: vokello@mksu.ac.ke (V.A.O.); vshikuku@kafuco.ac.ke (V.O.S.)

Abstract: Paraoxon is an emerging organophosphate pollutant that is commonly used as a pesticide and a drug, hence increasing the risk of contamination of water supplies. Its intensive use for vector control has led to pollutions in soil and water. Paraoxon is very toxic, with an LD_{50} of 2 to 30 mg/kg in rats. It can be metabolized in the body from parathion; thus, exposure can lead to serious health effects. In this study, zero valent iron (Fe°/ZVI NPs) nanoparticles were synthesized and investigated for the degradation of Paraoxon, a chemical warfare agent and insecticide, in an aqueous solution. The effects of solution pH, initial pollutant concentration, ZVI NPs dosage and contact time on mineralization efficiency were examined. Batch experiments demonstrated that 15 mg L^{-1} of Paraoxon was mineralized at degradation efficiencies of 75.9%, 63.9% and 48.9% after three-hour treatment with 6.0, 4.0 and 2.0% w/v Fe°, respectively. The calculated kinetic rate constant k_{obs} was 0.4791 h^{-1}, 0.4519 h^{-1} and 0.4175 h^{-1} after treating 10, 15 and 20 mg L^{-1} of Paraoxon solution with 6.0% w/v Fe, respectively. The degradation dynamics were described by the first-order kinetic law as evidenced by rate constants independent of the initial Paraoxon concentration. The degradation efficiency was strongly dependent on pH, increasing with a decrease in pH, with maximum removal at pH 4. p-nitrophenol was detected as a degradation product, suggesting cleavage of the O-P bond and hydrolysis as possible reaction processes. This study showed that Fe° particles have the potential for degrading Paraoxon.

Keywords: water remediation; reduction; degradation; Paraoxon; zero-valent iron; nanoparticles

Citation: Okello, V.A.; K'Owino, I.O.; Masika, K.; Shikuku, V.O. Reduction and Degradation of Paraoxon in Water Using Zero-Valent Iron Nanoparticles. *Sustainability* **2022**, *14*, 9451. https://doi.org/10.3390/su14159451

Academic Editor: Alessio Siciliano

Received: 31 March 2022
Accepted: 25 July 2022
Published: 2 August 2022

1. Introduction

Emerging pollutants have increased the concern of all stakeholders over the world due to their harmful potential state and ubiquitous presence in water, soil and air. Organophosphate compounds, in particular, comprise mainly of a very large class of chemical pesticides that are extensively used in agriculture worldwide [1]. These compounds comprise of methyl parathion, parathion, chlorpyrifos, malathion and Paraoxon [1,2]. The organophosphate compounds such as tabun, sarin, soman and cyclohexyl sarin have also been utilized as chemical-warfare agents (CWAs) in countries in the Western and Eastern bloc [3]. For example, Paraoxon, a renowned chemical warfare agent, has been widely utilized in South Africa as a biological nerve agent and is also used as an ophthalmological drug against glaucoma [4]. These compounds, when used, act by inactivating acetylcholinesterase, an essential ingredient for nerve function in insects, animals and humans; hence, they can also be used as a pesticide [5]. Unfortunately, Paraoxon is very unstable and is extremely toxic, and therefore, it should be removed from drinking water, as exposure can lead to vomiting, poor visions, convulsions, dyspnoea, lung oedema and even death. Moreover, with the dwindling amounts of fresh water available for human/animal consumption and agricultural use, the removal of toxins from these water bodies is of utmost importance.

There are a number of methods that have been used for the degradation of organophosphates from water with appreciable success [6–13]. Ghosh et al. [13] studied the hydrolysis of carboxylic esters such as Paraoxon using N- hydroxylamines and N- hydroxy amides in surfactants such as cationic micellar media. The degradation rate of substrates is enhanced by the presence of CTA (Cetyltrimethylammonium) surfactants in the case of both nucleophiles, N-hydroxysuccinimide and N-hydroxyphthalimide. Given their ability to support the rate enhancement of esterolytic reactions, they also provide the best means of solubilizing hydrophobic compounds in aqueous media. Therefore, the hydrolysis process is enabled, since N-hydroxy amides have structural similarity with hydroxamic acids with N-OH as functional groups [6]. However, the nucleophile reactivity in micelle depends on the fixation of the substrate and the reaction with anionic nucleophiles; thus, it is not an effective method [7].

Further studies by Chi et al. [8] used 4-nitrophenol surface-modified multiwalled carbon nanotubes for the sequestration of Paraoxon. The selective binding sites on the enzyme are made during polymer synthesis by the addition of a specific molecule as the template. However, this technique seemed to involve high capital investment to develop a highly selective enzyme, such as phosphotriesterase-immobilized polymers, thus limiting its application in the large-scale sequestration of Paraoxon. The molecular dynamics applying the combined quantum mechanical and molecular mechanical (QM/MM) potentials were also studied to determine the hydrolysis reaction mechanism of Paraoxon by phosphotriesterase (PTE) [9].

In other studies, microbial degradation approaches were considered to offer reliable and inexpensive ways to safely eliminate Paraoxon from both terrestrial and aquatic environments [10]. These frontiers have resulted in the identification of bacterial strains and enzymes that are capable of detoxifying organophosphate pesticides. The study by Wu et al. [10] noted that the immobilized organophosphorus hydrolase (OPH) enzyme isolated from Pseudomonas diminuta MG and Flavobacterium sp. ATCC 27551 was capable of degrading Paraoxon. Catalysis of this Paraoxon is by hydrolyzing phosphorus ester bonds, such as P-O and P-S bonds, through a hydrolytic mechanism that involves adding an activated water molecule at the phosphorus center [11]. More so, E. coli has been utilized to mineralize Paraoxon by co-expression of organophosphorus hydrolase (OPH) under *trc* promoter and *Vitreoscilla* hemoglobin (VHb) under the O_2-dependent *nar* promoter [12]. Additionally, a strain of Pseudomonas putida was constructed, which was seen to efficiently degrade Paraoxon and utilize it as an energy source. This strain was catalyzed with the *pnp* operon from Pseudomonas sp. strain ENV2030, which incorporated enzymes that convert p-nitrophenol into β-ketoadipate. Due to the large extent of the polluted environment, chemical and enzyme preparation strategies seemed inappropriate, as they are uneconomical.

Phytoremediation has also been proposed as a potentially cheap, efficient and an environmentally benign approach to be used for degradation of organophosphates such as Paraoxon and methyl parathion. Presently, there is a growing interest in the use of nanoparticles in the degradation of toxic organic compounds from the environment [14]. Prasad et al. [15] reported the photocatalytic destruction of Paraoxon-ethyl in aqueous solution using titania nanoparticulate film. The study showed that titania nanoparticles degrade Paraoxon-ethyl to form silylated products, which include p-nitrophenol, O,O-diethyl phosphonic acid, O-ethyl diphosphonic acid and phosphoric acid as by-products. These products form due to the cleavage of P–O–C bonds and oxidation of the P atom. Despite its effectiveness, recovery of the spent TiO_2 photocatalyst from solutions is costly and technologically prohibitive.

Elsewhere, Xiudong et al. [16] used nanocrystalline magnesia powder (nano-MgO) on the degradation of Paraoxon. However, the catalytic activity relies on the availability of light. The two micellized ion complexes, Co(II) and Cr(III), possessed fine catalytic activity in mineralizing Paraoxon. These metal ions polarize the P = O group, since micellization facilitates reduction and also promotes the electrophilicity of the metal towards the micelle-

bound substrate [6]. Bromberg and co-workers [17] reported the use of functionalized silver and cobalt nanoparticles for Paraoxon hydrolysis. In other studies, the use of core/shell molecular imprinting microparticles fabricated using reversible addition-fragmentation transfer polymerization (RAFT) technology was developed for the degradation of Paraoxon. However, this technology requires the use of phosphotriesterase to catalyze the hydrolysis reaction for the degradation of Paraoxon [18]. Furthermore, these methods are very expensive to use, and recovery of the complexes from the environment remains a challenge. Therefore, there is a need to develop other suitable and convenient methods to completely eradicate the toxic Paraoxon pesticide from the environment.

With the limited studies on the degradation of Paraoxon reported in literature and the postulated limitations, alternative treatment procedures should thus be developed. Therefore, we hereby report the possible application of zero-valent iron nanoparticles (ZVI NPs) in the degradation of the toxic organophosphorus compound, Paraoxon, in aqueous media into non-toxic materials under room temperature batch experiment conditions. Moreover, to the best of our knowledge, no study has reported on the degradation of Paraoxon using ZVI NPs. These particles were selected because they have been preferably used to transform a plethora of environmental pollutants, such as chlorinated hydrocarbons and pesticides, etc., under reduction reactions or sorption processes. This is due to their increased surface area, fast reaction, low cost and availability [19]. The ZVI NPs are excellent electron donors and have a high potential to reduce various contaminants. This study, therefore, evaluated the capability of ZVI NPs to degrade Paraoxon in water as a function of the Paraoxon initial concentration, ZVI NPs dosage, solution pH and contact time. The results indicate a great potential in the use of ZVI NPs for the degradation of Paraoxon in water.

2. Materials and Methods

Paraoxon Standard was obtained from Dr. Ehrenstorfer GmbH (Augsburg, Germany). Acetonitrile (HPLC grade, 98.0% purity), Sodium Borohydride, Ethanol and Ferric Chloride Hexahydrate were all analytical grade, obtained from Kobian Company Ltd. A stock solution of 1000 mg L^{-1} Paraoxon in acetonitrile was prepared. Solutions of varying concentrations (1, 5, 10, 15, 20 and 25 mg L^{-1}) were prepared by serial dilution of the stock solution using acetonitrile. The effect of Fe° dosage was evaluated using 2.0, 4.0, 6.0, 8.0 and 10.0% *w*/*v* dosages for a fixed initial Paraoxon concentration. All aqueous solutions were made with ultra-high-purity water, obtained using an ultrapure water system Milli-Q Plus (Merck Millipore Co., Darmstadt, Germany).

2.1. Preparation of ZVI NPs

The preparation of solutions involved dissolving 9.4575 g of sodium borohydride ($NaBH_4$) in 0.1 M NaOH solution and then 12.1635 g of $FeCl_3 \cdot 6H_2O$ into 100 mL of ethanol/water mixture [20]. The stabilized ZVI NPs were prepared adding 0.25 M $NaBH_4$ aqueous solution dropwise to a Neon gas-purged 0.045 M $FeCl_3 \cdot 6H_2O$ aqueous solution in the ratio of 1:1 at 23 °C with magnetic stirring. The solution was magnetically stirred for 20 min, then centrifuged for 2 min, and the supernatant solution was replaced with acetone. The ZVI NPs were finally washed with 25 mL of absolute ethanol, then stored in a refrigerator at <4 °C.

2.2. Characterization of Zero Valent Iron Nanoparticles

2.2.1. Transmission Electron Microscopy (TEM) Analysis

The images (size and shape) of iron nanoparticles were obtained using 4q TEM JEOL equipment equipped with a LaB6 model filament set at an acceleration of 200 kV and beam current of 102 µA.

2.2.2. Scanning Electron Microscopy (SEM) Analysis

The Scanning Electron Microscopy (SEM) analysis was done using the Philips XL30 SEM machine (F.E.I. Company, Hillboro, OR, USA) to inspect the surface morphology. The sample surface images were taken at different magnifications.

2.3. Batch Experiments

Here, separate 50 mL of 15 mg L^{-1} Paraoxon solutions were mixed with 2.0, 4.0 and 6.0% w/v of ZVI NPs (Fe°). For study of the effect of pH on Paraoxon destruction, the pH of Paraoxon solutions containing the nanoparticles were adjusted to 10, 7 and 4. The effect of initial Paraoxon concentration (10, 15 and 20 mg L^{-1}) on degradation rate was studied using 6.0% w/v Fe° dosage at 22 °C. At pre-determined time intervals, 2 mL of aliquot was withdrawn from the reaction vessel, centrifuged at 3000 rpm and analyzed for the residual Paraoxon concentration using a Shimadzu UV-Vis Spectrophotometer (Model 1601 by ThermoFisher Scientific, Randburg, South Africa) at a wavelength of 280 nm.

The Paraoxon degradation kinetics were modeled with a first-order rate equation (Equation (1)) with the residual concentration of Paraoxon measurements made at pre-determined time intervals for 3 h.

$$\frac{d[paraoxon]}{dt} = -k_{obs}[paraoxon] \quad (1)$$

where [*paraoxon*] is the concentration of Paraoxon in the aqueous solution (mg L^{-1}), t is time t (min) and k_{obs} is the first-order rate constant (min^{-1}).

2.4. Analytical Methods

A chromatographic analysis was performed using an HPLC system, Shimadzu LC-20AT, equipped with an SPD-20A Shimadzu prominence UV/visible detector, degasser (DGU-20A prominence, Shimadzu) and Phenomenex 00 G-4420-E0 (250 £ 4.60 mm, 5 microns, HyperClone 5u BDS C-18 130A) columns. The mobile phase was Acetonitrile:water (1:1) at a flow of 0.7 mL/min, detector wavelength of 254 nm and an injection volume of 20 µL. The equipment was purchased from LAB2, Berkel en Rodenrijs, The Netherlands.

Quality Control

For quality control, reagents and materials used were either HPLC grade or analytical grade, unless stated otherwise. Data were obtained from triplicate analyses and processed using Microsoft Excel (5.0/95 workbook by Microsoft Office, TDK solutions Ltd, Nairobi, Kenya) and OriginPro 9.0 software (OriginLab Corporation, Northampton, MA, USA).

3. Results and Discussion

3.1. Characterization of Zero Valent Iron Nanoparticles

3.1.1. Transmission Electron Microscopy (TEM)

Generally, the removal of Paraoxon and/or other pollutants from water is highly dependent on the shape and size of the nanoparticle used, hence the need to perform morphological characterization of the ZVI NPs. Figure 1 displays the sizes of the iron nanoparticles after being characterized using TEM. The cumulative size distribution average of the nanoparticles confirmed that the NPs with less than 100-nm diameters constituted more than 80.0%, while particles with less than 60 nm size accounted for less than 50.0%. The fabricated nanoparticles showed chain-like hollow structures, the majority of which ranged between 20 nm–90 nm diameter. It is believed that these aggregated to remain in the most thermodynamically stable state [21].

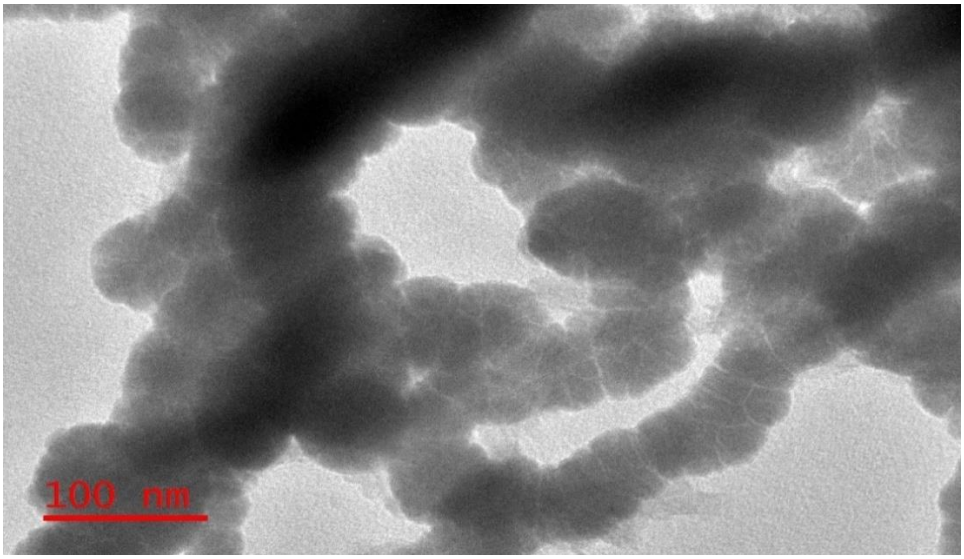

Figure 1. TEM images of freshly prepared ZVI NPs (100 nm) showing a network of chain-like hollow structures.

3.1.2. Scanning Electron Microscopy (SEM)

The SEM micrograph for the particles after contact with Paraoxon is presented in Figure 2. It depicts the formation of large agglomerates with highly irregular surfaces, containing large and small intertwined agglomerates [22]. The surface morphology of freshly prepared ZVI NPs changed greatly after the interaction with Paraoxon into white islands of porous spherical particles. The latter was attributed to the dissociative adsorption of water and Paraoxon into the hollow porous sites, which served as reaction sites for the ensuing reduction. In this case, the iron surface Fe^0 released electrons to the water, resulting to the formation of surface-fixed hydroxyl moieties that created highly reducing conditions for Paraoxon, as indicated in the following equations. Equation (2) indicates the reaction of ZVI NPs with dissolved oxygen in water to form hydrogen peroxide, which was subsequently reduced to water (Equation (3)) or to hydroxyl radicals (Equation (4)). The latter reaction is responsible for the degradation of Paraoxon, as shown in Scheme 1.

$$Fe^{\circ} + O_2 + 2H^+ \rightarrow Fe^{2+} + H_2O_2 \quad (2)$$

$$Fe^{\circ} + H_2O_2 + 2H^+ \rightarrow Fe^{2+} + 2H_2O \quad (3)$$

$$Fe^{2+} + H_2O_2 \rightarrow Fe^{3+} + \cdot OH + OH^- \quad (4)$$

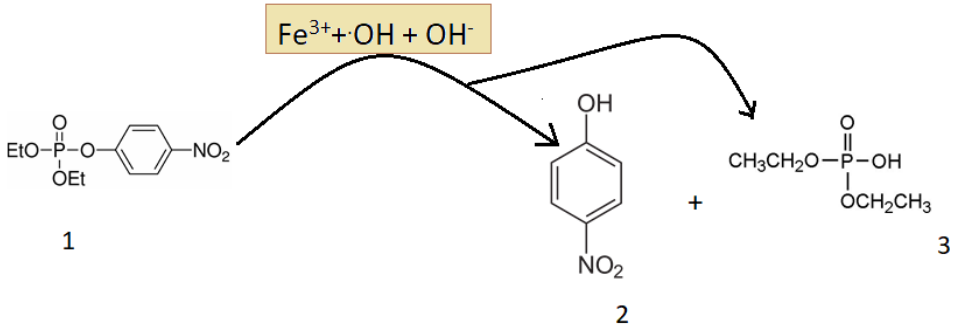

Scheme 1. Degradation mechanism of Paraoxon (**1**) by the hydroxyl radicals to form p-nitrophenol (**2**) and O,O-diethyl phosphate (**3**).

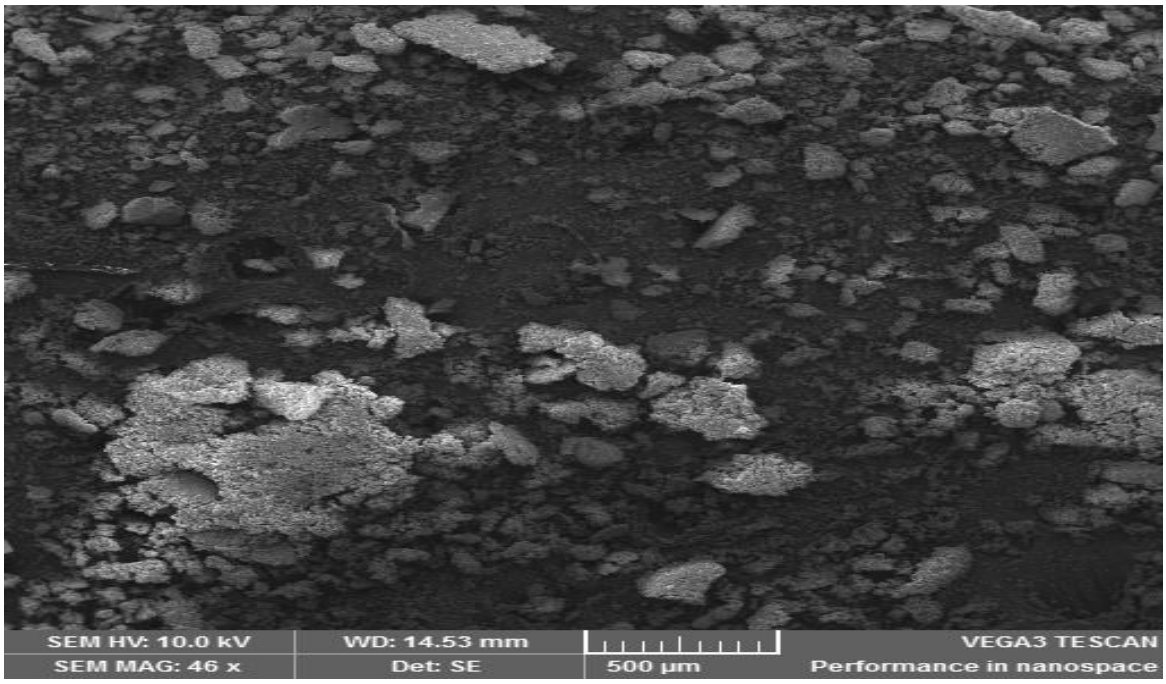

Figure 2. The SEM images of Fe° nanoparticles after incubation with Paraoxon.

3.1.3. Energy Dispersive X-ray Analysis (EDXA)

EDXA is an X-ray technique that is used in the identification of the elemental composition of materials. The EDXA image obtained before subjecting the particles to Paraoxon is as shown in Figure S1. The characteristic broad peaks in Figure S1 indicated a sufficient presence of zero-valent iron in the sample. EDXA spectrum Figure 3a,b shows the elemental analysis of ZVI NPs after incubation with Paraoxon. The result analysis shows that ZVI NPs consist of 76.2% of iron, 22.7% of oxygen, 0.5% of silicon, 0.2% of uranium, 0.1% of tin, 0.1% of lead, 0.2% of thorium and 0.1% of aluminum. These results confirmed the presence of different metal elements in the synthesized ZVI NPs with high amounts of Fe (76.2%).

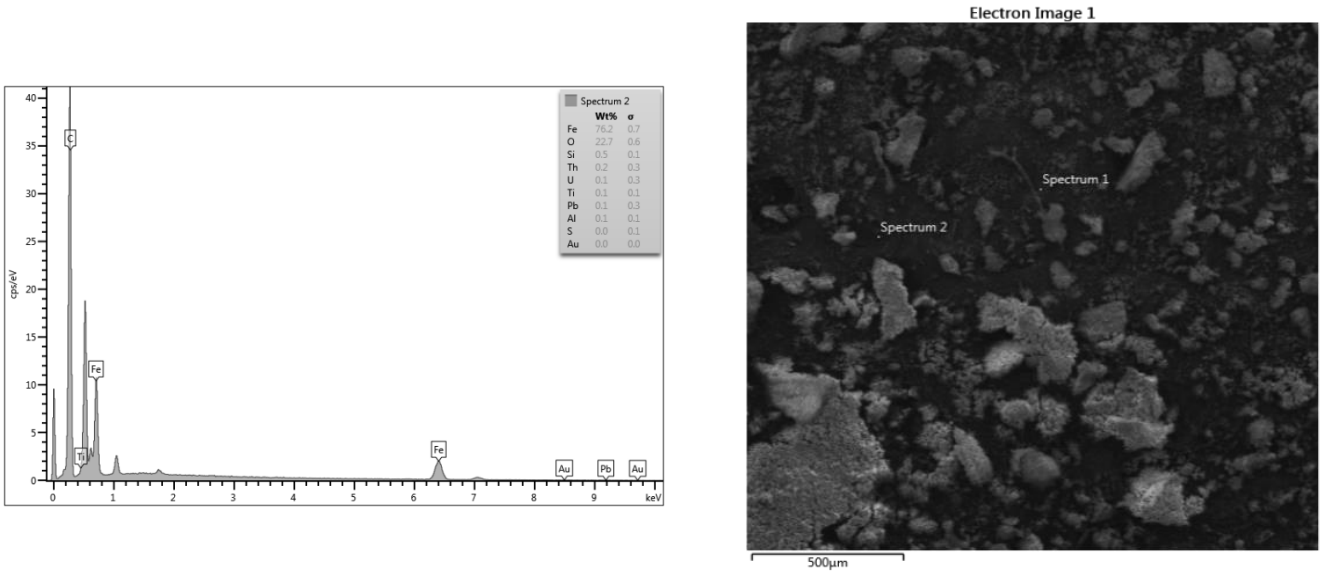

(**a**) (**b**)

Figure 3. (**a**) Energy Dispersive X-ray Analysis (EDXA) image of zero-valent iron NPs after incubation with Paraoxon. (**b**) SEM image showing the crystallinity of ZVI NPs.

3.2. Degradation kinetics of Paraoxon

3.2.1. Effect of Time on the Degradation of Paraoxon

The rate of disappearance of Paraoxon with time, in the presence and absence of Fe° NPs, was monitored over a three-hour period. The results, shown in Figure 4, demonstrated that 63.5% mineralization of Paraoxon was attained in 3 h in the presence of Fe° NPs at 2.0% *w*/*v* dosage. Contrarily, without Fe° NPs (control), no appreciable degradation (<2.0%) of Paraoxon was realized, indicating the effectiveness of Fe° NPs in the sequestration of Paraoxon under these conditions.

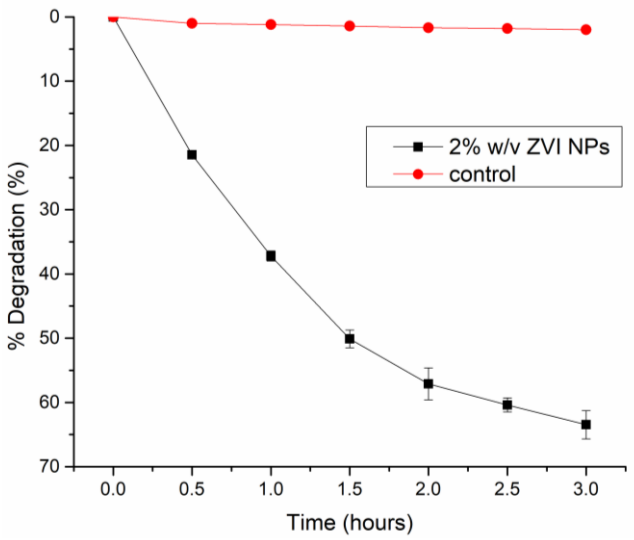

Figure 4. Percent degradation of Paraoxon with time (C_o = 15 mg L^{-1}, dosage = 2.0% *w*/*v* ZVI NPs). The error bars reflect the standard deviation of three repeat experiments.

3.2.2. Effect of Nano Zero Valent Iron (Fe°) Dosage on Degradation Efficiency

The study on the effect of Fe° dosage on degradation efficiency was evaluated. From Figure 5, an increase in Fe° dosage, from 2.0% *w*/*v* to 6.0% *w*/*v*, significantly ameliorated the degradation efficiency of Paraoxon from 63.5% to 85.8%, respectively. The rapid initial degradation rate of Paraoxon was attributed to the presence of a large number of energetically favorable catalytic sites. However, beyond 6.0% *w*/*v* dosage, there was no appreciable change in percent degradation due to overlapping of the active sites as a result of agglomeration of the ZVI particles. A dosage of 6.0% *w*/*v* was realized as the optimum.

The change in the concentration of Paraoxon is attributed to both degradations to other metabolites and adsorption. A mass balance analysis was beyond the scope of the present work. The zero valent iron nanoparticles reacted with oxygen to form Fe^{2+} and O_2^{2-}. The O_2^{2-} formed reacts with hydrogen to form hydrogen peroxide, which then reacts with Fe^{2+} to form Fe^{3+} and hydroxyl radicals, which are highly reactive oxidants. The hydroxyl radicals initiate a nucleophilic attack on the phosphorus center by cleaving the P-O-C bond to produce 4-nitrophenol as a major by-product, which is eventually mineralized through further oxidation. The Fe^{3+} generated will be precipitated out as hydroxides [19]. See Equations (1)–(3) in Section 3.1.2.

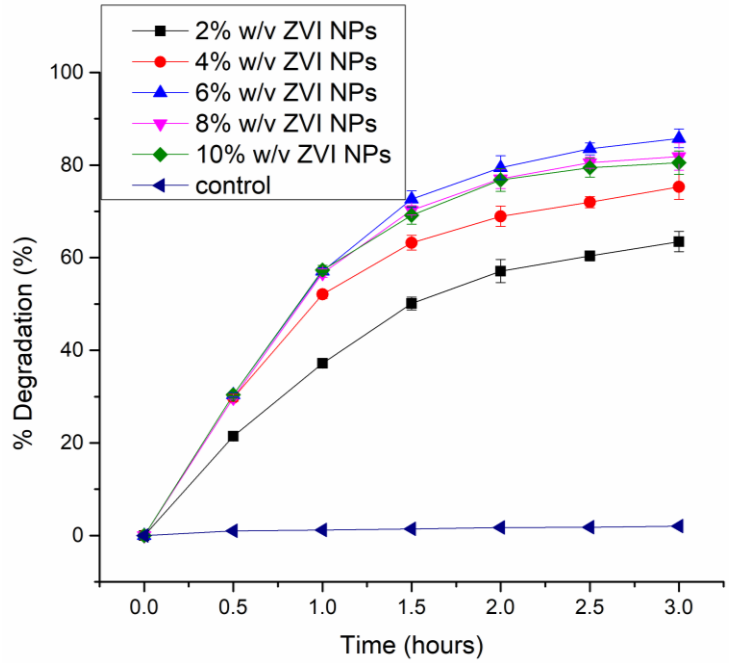

Figure 5. Effect of ZVI NPs dosage on Paraoxon degradation. The error bars reflect the standard deviation of three repeat experiments.

3.2.3. Effect of pH on Paraoxon degradation

The effect of solution pH on Paraoxon degradation was examined at pH 4, 7 and 10, holding other conditions constant. The observed degradation efficiency of Paraoxon increased significantly ($p < 0.05$) with a decrease in solution pH with a maximum removal at pH 4 (Figure 6). This trend indicates that the efficiency of zero valent iron nanoparticles to degrade Paraoxon was influenced by H^+ ions. Similar observation was reported by Li et al. [23] for the degradation of acid orange 7 dye using nanoscale zero valent iron.

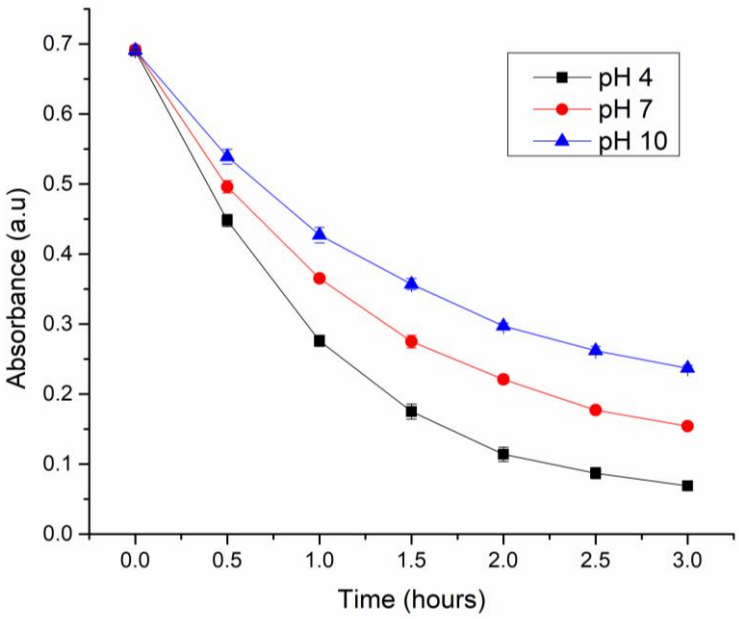

Figure 6. Effect of pH on Paraoxon degradation. The error bars reflect the standard deviation of three repeat experiments.

3.2.4. Effect of Nano Zero Valent Iron (Fe°) Dosage on Degradation Kinetics

The Paraoxon degradation kinetics were modeled with a first-order rate equation (see Equation (1)), since degradation processes are typically first-order reactions. The suitability of the model was inspected using the coefficient of determination (R^2) values.

The rate constants (k_{obs}) were determined by linear regression of the experimental data following the first-order rate equation. The value of k_{obs}, calculated from Figure 7, was 0.2245 h^{-1}, 0.3354 h^{-1} and 0.4800 h^{-1} for 2.0% w/v, 4.0% w/v and 6.0% w/v of ZVI NPs, respectively. This proved that the rate of degradation was enhanced with the increased ZVI NPs dosage consistent with the observed increased removal efficiency previously discussed. The high coefficients of determination (R^2) values indicate that the degradation kinetics followed the first-order kinetic law.

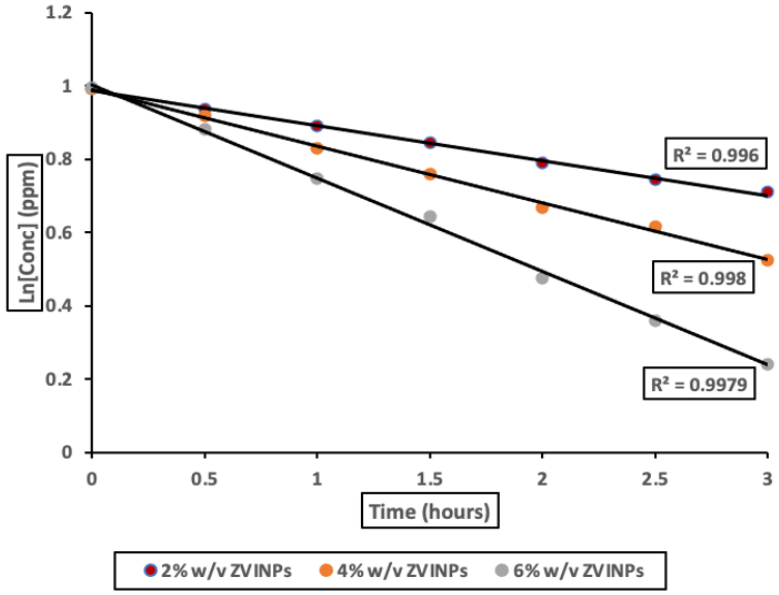

Figure 7. Paraoxon degradation first-order linear regression plots.

3.2.5. Effect of Paraoxon Initial Concentration on Degradation Kinetics

The effect of initial Paraoxon concentration (10, 15, and 20 mg L^{-1}) on the degradation kinetics was investigated at a fixed Fe° dosage (6.0% w/v) and also to verify the validity of the previously affirmed conclusion that degradation of Paraoxon in the presence of Fe° is a first-order reaction. The experimental data showed high linearity when tested against the first-order kinetics equation (Figure 8). The corresponding calculated k_{obs} values were 0.0074 h^{-1}, 0.0073 h^{-1} and 0.0069 h^{-1} for initial concentrations of 10, 15 and 20 mgL^{-1}, respectively. These values denote that the degradation half-life of Paraoxon is independent of the initial concentration. This confirms the degradation dynamics for the first-order kinetics.

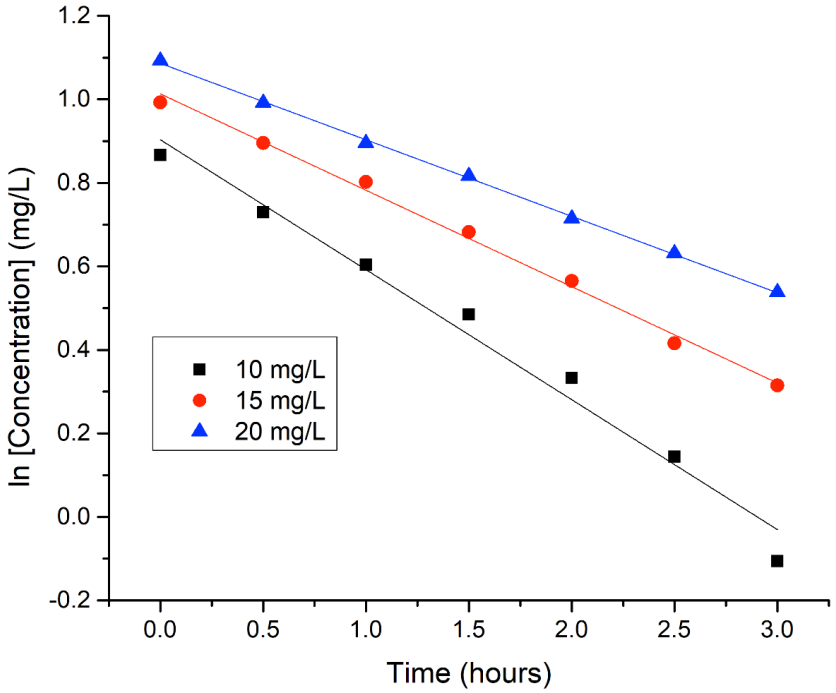

Figure 8. First-order linear regressions plots for Paraoxon at different initial concentrations (dose = 6.0% *w*/*v* ZVI NPs).

3.3. Degradation Products of Paraoxon

As aforementioned, ZVI NPs have been used extensively for the remediation of contaminated soil and groundwater. This is due to their large active surface area; hence, they serve as strong and effective reductants for environmental pollutants. We further, investigated this fact using HPLC, in which the reduction in Paraoxon peak was monitored with time. The residual Paraoxon and metabolites after incubation of Paraoxon with ZVI NPs for 0 to 3 h was determined by noting their respective retention time. Paraoxon was detected at a retention time of 24.1 min and a degradation product at 10.6 min. Qualitatively, chromatogram peaks for Paraoxon and p-nitrophenol standards coincided with the retention times for those of Paraoxon, and the metabolite peak formed after the degradation process, suggesting that the by-product formed was p-nitrophenol. As seen in Figure 9, the emergence of the metabolite peak, p-nitrophenol, is followed by a consistent increase of this peak with time and concomitant decrease in the Paraoxon peak.

The findings in Figure 9 were complemented further by Uv-Visible spectroscopy results (Figure S2). In this case, the addition of ZVI NPs to Paraoxon caused a decrease in the absorption peak intensity at 270 nm with time, with a concomitant gradual increase in intensity with time of a new band observed at ~310 nm. The decrease in the Paraoxon peak intensity at 270 nm was as a result of cleavage of the O-P bond and formation of new product(s) (Scheme 1). This is supported by an isosbestic point observed at ~295 nm (Figure S2) that gives credence to a new species forming during the interaction between the Paraoxon and the ZVI NPs.

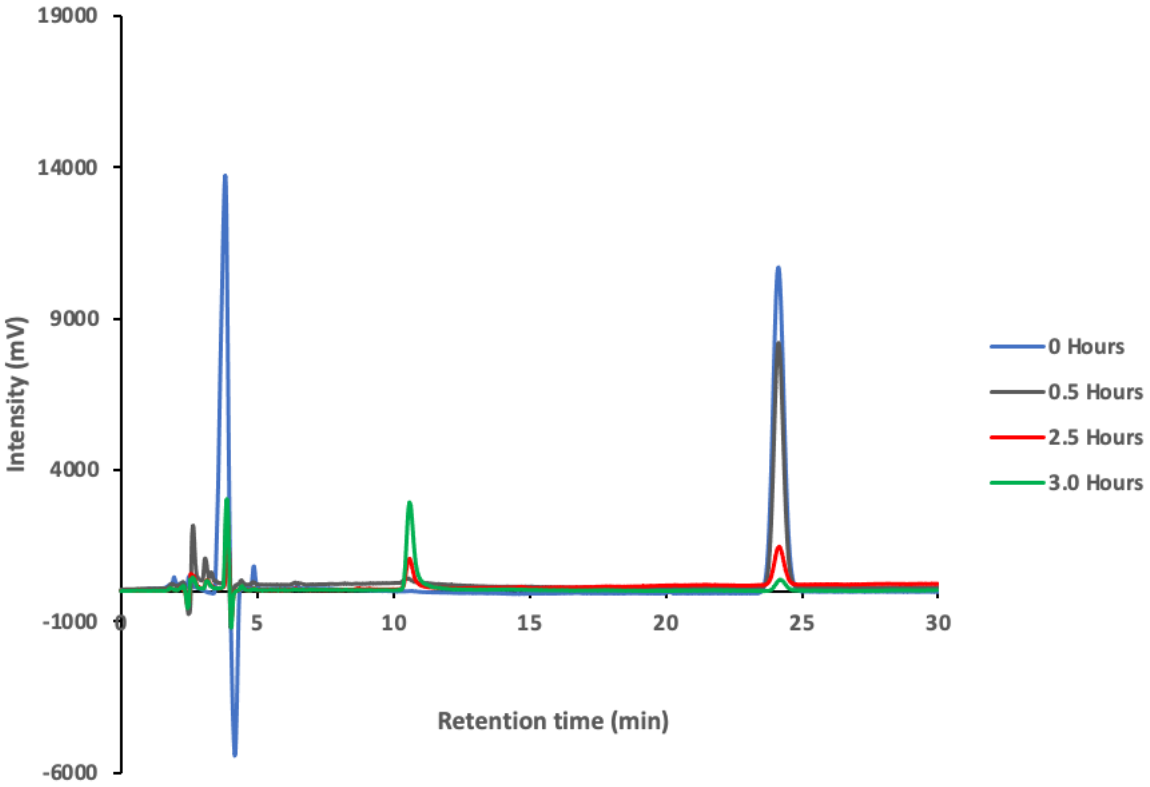

Figure 9. Chromatograms showing Paraoxon and its metabolite (p-nitrophenol) peak after various hours of incubation of ZVI NPs with 15 mg mL^{-1} Paraoxon.

The mechanism of degradation of Paraoxon is shown in Scheme 1. In this case, the hydroxyl radical and hydroxyl ions reacted with the Paraoxon (1) molecules to induce the cleavage of the O-P bond to p-nitrophenol (2) and O,O-diethyl phosphate (3). This proposed mechanism is premised on a number of studies [24,25] that have proven that compounds 2 and 3 are products of hydroxyl degradation of Paraoxon. Thus, while the present study highlights the degradation of Paraoxon to p-nitrophenol by Fe° NPs, it highly possible that other degradation products, such as O,O-diethyl phosphate, undetected herein by the HPLC method were formed.

4. Conclusions

The degradation of Paraoxon, an organophosphate-based chemical warfare agent and an emerging environmental pollutant, was investigated using ZVI NPs. The results demonstrated that the ZVI NPs are capable of degrading Paraoxon in water. However, characterization of the ZVI NPs before and after sorption of paraoxon shows that these nanoparticles undergo several surface changes after the sorption process, as indicated by the TEM and SEM images obtained. The effects of solution pH, initial pollutant concentration, ZVI dosage and contact time on mineralization efficiency were investigated. Batch experiments demonstrated that Paraoxon was mineralized at degradation efficiencies that were dependent on treatment time, pH and amount of the ZVI NPs. The optimum degradation of Paraoxon was 6.0% w/v ZVI NPs, with an efficiency of 75.9%. The degradation of Paraoxon pesticide is strongly pH-dependent, with enhanced degradation efficiency observed at pH 4. Paraoxon degradation followed first-order kinetics, indicated by the high coefficients of determination and independence of the rate constant to initial Paraoxon concentration.

This study shows that ZVI NPs potentially offer an alternative method for the destruction of Paraoxon from the aqueous environment, subject to further investigations in real environmental water samples. Given the high value of nanoparticles and that nanosized materials can impact human health, in addition to presenting environmental, separation,

recovery and reuse problems, further investigations on the possible recycling of the ZVI NPs are necessary.

Supplementary Materials: The following supporting information can be downloaded at: https://www.mdpi.com/article/10.3390/su14159451/s1, Figure S1: Energy Dispersive X-ray Analysis (EDXA) image of freshly prepared zero-valent iron NPs. Figure S2. Evolution of Paraoxon concentration with time after incubation of 15 mg L^{-1} of Paraoxon with 2% ZVI NPs for 3 h.

Author Contributions: Conceptualization, V.A.O. and I.O.K.; methodology, V.A.O. and I.O.K.; software, V.A.O. and V.O.S.; validation, V.A.O., I.O.K. and V.O.S.; formal analysis, K.M.; investigation, K.M.; resources, V.A.O. and I.O.K.; data curation, V.O.S.; writing—original draft preparation, K.M.; writing—review and editing, was done by all the authors; visualization, V.A.O. and I.O.K.; supervision, V.A.O. and I.O.K.; project administration, V.A.O. and I.O.K.; funding acquisition, V.A.O. and I.O.K. All authors have read and agreed to the published version of the manuscript.

Funding: This research was funded by the National Commission of Science, Technology and Innovation, Kenya, under Grant number (NCST/5/003/3rd CALL MSc/026). The APC was not funded but was paid from personal finances.

Institutional Review Board Statement: Not applicable.

Informed Consent Statement: This article does not contain any studies involving human or animal subjects.

Data Availability Statement: Not applicable.

Acknowledgments: This work was supported by the National Commission of Science, Technology and Innovation, Kenya, under Grant number (NCST/5/003/3rd CALL MSc/026). We recognize the contribution of Selly Kimosop, Daniel Onunga, Manoah Opanga and Agnes Muyale towards the completion of this work.

Conflicts of Interest: The authors declare that there are no conflict of interest.

References

1. Kaushal, J.; Khatri, M.; Arya, K. A treatise on Organophosphate pesticide pollution: Current strategies and advancements in their environmental degradation and elimination. *Ecotoxicol. Environ. Saf.* **2021**, *207*, 111483. [CrossRef] [PubMed]
2. Soares, S.; Birolli, G.; Ferreira, M.; Porto, M. Biodegradation pathway of the organophosphate pesticides chlorpyrifos, methyl parathion and profenofos by the marine-derived fungus Aspergillus sydowii CBMAI 935 and its potential for methylation reactions of phenolic compounds. *Mar. Pollut. Bull.* **2021**, *166*, 112185. [CrossRef] [PubMed]
3. Hrvat, N.; Kovarik, Z. Counteracting poisoning with chemical warfare nerve agents. *Arch. Ind. Hyg. Toxicol.* **2020**, *71*, 266–284. [CrossRef]
4. Zhang, X.; Feng, Y.; Li, J.; Ai, D.; Xi, G.; Zhao, M. Electrochemical Nonenzymatic Sensor Based on $NiOFe_2O_3$@carbon Nanotubes Nanocomposite for Determination of Paraoxon in Fruits and Water. *Int. J. Electrochem. Sci.* **2021**, *16*, 210711. [CrossRef]
5. Kitagawa, S.; Cavalcante, F.; de Paula, L.; Rodrigues, B.; Bernardo, B.; da Silva, C.J.; da Silva, N.; dos Santos, V.; Granjeiro, M.; de Almeida, S. In Vitro Evaluation of Neutral Aryloximes as Reactivators for Electrophorus eel Acetylcholinesterase Inhibited by Paraoxon. *Biomolecules* **2019**, *9*, 583. [CrossRef] [PubMed]
6. Hafiza, A.A.; El Awadia, Y.M.; Badawia, M.A.; Mokhtar, M.S. Catalytic Destruction of Paraoxon by Metallomicelle Layers of Co(II) and Cr(III)., Paper no. S1447. *J. Surfactants Deterg.* **2005**, *8*, 203–206. [CrossRef]
7. Mello, V.S.; Coutures, C.; Leblanc, M.R.; Cheng, T.; Rastogi, K.V.; DeFrank, J.J. Interaction between organophosphorus hydrolase and Paraoxon studied by surface chemistry in situ at air-water interface. *Chemosphere* **2001**, *55*, 881–887.
8. Chi, W.; Shi, H.; Shi, W.; Guo, Y.; Guo, T. 4-Nitrophenol surface molecularly imprinted polymers based on multiwalled carbon nanotubes for the elimination of Paraoxon pollution. *J. Hazard. Mater.* **2012**, *228*, 243–249. [CrossRef] [PubMed]
9. Wong, K.; Gao, J. The Reaction Mechanism of Paraoxon Hydrolysis by Phosphotriesterase from Combined QM/MM Simulations. *Biochemistry* **2007**, *46*, 13352–13369. [CrossRef]
10. Wu, C.; Cha, J.H.; Valdes, J.J.; Bentley, E.W. GFP-Visualized immobilized Enzymes degradation of Paraoxon via organophosphorus Hydrolase in a packed column. *Biotechnol. Bioeng.* **2000**, *77*, 212–218. [CrossRef] [PubMed]
11. Grimsley, K.J.; Calamini, B.; Wild, R.J.; Mesecar, D.A. Structural and mutational studies of organophosphorus hydrolase reveal a cryptic and functional allosteric-binding site. *Arch. Biochem. Biophys.* **2005**, *442*, 169–179. [CrossRef] [PubMed]
12. Kang, G.D.; Kim, H.Y.J.; Cha, J.H. Enhanced detoxification of organophosphates using recombinant *Escherichia coli* with co-expression of organophosphorus hydrolase and bacterial hemoglobin. *Biotechnol. Lett.* **2002**, *24*, 879–883. [CrossRef]

13. Singh, N.; Karpichev, Y.; Sharma, R.; Gupta, B.; Sahu, K.; Satnami, L.; Ghosh, K.K. From α-nucleophiles to functionalized aggregates: Exploring the reactivity of hydroxamate ion towards esterolytic reactions in micelles. *Org. Biomol. Chem.* **2015**, *13*, 2827–2848. [CrossRef]
14. Rao, W.; Lv, G.; Wang, D.; Liao, L. Enhanced Degradation of Rh 6G by Zero Valent Iron Loaded on Two Typical Clay Minerals with Different Structures Under Microwave Irradiation. *Front. Chem.* **2018**, *6*, 463. [CrossRef]
15. Prasad, K.G.; Ramacharyulu, K.R.P.V.; Praveen Kumar, J.; Srivastava, R.A.; Singh, B. Photocatalytic degradation of Paraoxon-ethyl in aqueous solution using titania nanoparticulate film. *Thin Solid Film.* **2012**, *520*, 5597–5601. [CrossRef]
16. Xiudong, Y.; Mengfu, Z.; Hongbo, Z.; Ping, C.; Cheng, D. Study on antibacterial efficacy and catalytic capability of nanocrystalline magnesia. *Adv. Mater. Res.* **2011**, *335*, 515–518.
17. Bromberg, L.; Chen, L.; Chang, P.E.; Wang, S.; Hatton, T. Reactive Silver and Cobalt Nanoparticles Modi fied with Fatty Acid Ligands Functionalized by Imidazole Derivatives. *J. Chem. Mater.* **2010**, *22*, 5383–5391. [CrossRef]
18. Guo, Y.; Yang, Y.; Zhang, L.; Guo, Y.T. Core/shell molecular imprinting microparticles using RAFT technology for degradation of Paraoxon. *Macromol. Res.* **2011**, *19*, 1202–1209. [CrossRef]
19. Li, Q.; Chen, Z.; Wang, H.; Yang, H.; Wen, T.; Wang, S.; Wang, X. Removal of organic compounds by nanoscale zero-valent iron and its composites. *Sci. Total Environ.* **2021**, *792*, 148546. [CrossRef]
20. El-Shafei, M.M.; Hamdy, A.; Hefny, M.M. Zero-valent iron nanostructure: Synthesis, characterization and application. *J. Environ. Biotechnol.* **2018**, *7*, 1–10.
21. Lin, Y.; Tseng, H.; Wey, M.; Lin, M. Characteristics of two types of stabilized nano zero-valent iron and transport in porous media. *Sci. Total Environ.* **2010**, *408*, 2260–2267. [CrossRef]
22. Talebzadeh, S.; Forato, F.; Bujoli, B.; Trammell, A.; Grolleau, S.; Pal, H.; Queffélec, C.; Knight, D. Non-photochemical catalytic hydrolysis of methyl parathion using core–shell Ag@TiO_2 nanoparticles. *RSC Adv.* **2018**, *8*, 42346–42352. [CrossRef]
23. Li, H.; Wan, J.; Ma, Y.; Wang, Y.; Huang, M. Influence of particle size of zero valent iron and dissolved silica on the reactivity of activated persulfate for degradation of acid orange 7. *Chem. Eng. J.* **2014**, *237*, 487–496. [CrossRef]
24. Wu, C.; Linden, G. Degradation and Byproduct Formation of Parathion in Aqueous Solutions by UV and UV/H_2O_2 Treatment. *Water Res.* **2008**, *42*, 4780–4790. [CrossRef]
25. Zhan, S.; Tseng, W.; Tseng, W. Impact of nanoceria shape on degradation of diethyl Paraoxon: Synthesis, catalytic mechanism, and water remediation application. *Environ. Res.* **2020**, *188*, 109653. [CrossRef]